Photopolymerized Patterning and Materials to Enhance Neural Prosthetic Performance

Bradley W. Tuft[1], Linjing Xu[2], Austin Hangartner[1], Scott White[1], Marlan Hansen[2], and Allan Guymon[1]

1. University of Iowa, Department of Chemical and Biochemical Engineering, Iowa City, IA

2. University of Iowa Hospitals and Clinics, Department of Otolaryngology, Iowa City, IA

ABSTRACT

Performance of successful neural prosthetics, such as the cochlear implant (CI), has not significantly improved in recent years due to poor spatial resolution at the nerve-implant interface. Directing neurites towards target electrodes may reduce problematic signal spread and improve stimulatory specificity. Consequently, our work utilizes the spatial and temporal control inherent to photopolymerization methodology to fabricate micropatterned methacrylate polymers that direct nerve cell growth based on substrate topographic and stiffness cues. Micropatterned substrates are formed in a rapid, single-step reaction by selectively blocking initiating light with glass-chrome photomasks which have repeating line-space features with a pitch of 10-100 μm in width. The resultant pattern is a continuous series of ridges and grooves at regular intervals that can be used for cellular contact guidance studies. Micro-feature depth is controlled and reproducibly generated from 220±40 nm to 16±1.3 μm by shuttering the light source at different time steps during the reaction and by modulating photo-initiator concentration. The ultimate goal of the research is to develop materials that predictably orient regenerative nerve cell growth and improve neural prosthetic stimulatory specificity and, thus, improve patient outcomes.

INTRODUCTION

Neural prostheses electrically stimulate neural tissue to restore or augment remaining motor and sensory functions of neural pathways that were lost or damaged due to disease or physical trauma. However, commercially available prostheses such as the cochlear implant and promising developmental prostheses such as the retinal implant suffer from poor spatial signal resolution which limits their ultimate performance.[1-3] For example, retinal prosthesis simulation is limited to few sensory pixels due, in part, to electrical signal overlap among target neurons in the retina caused by spatial separation of stimulating electrodes from the neural tissue.[3] The CI enables basic speech perception but suffers from comparable spatial signaling limitations due to nonspecific excitation of neurons within the cochlea which preclude high fidelity tonal simulation for the user (Fig 1). Subsequently, CI patients struggle with complex auditory stimuli such as voice comprehension in noisy environments and music appreciation.[4,5]

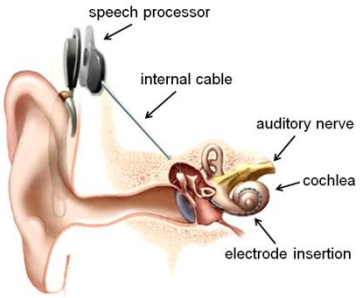

Figure 1. Representation of the cochlear implant (CI). The CI provides auditory perception to individuals with severe hearing loss and is currently the most successful neural prosthetic.

Driving regenerative neural processes into closer spatial proximity of specific stimulating electrodes would allow for lower current trigger thresholds that would reduce problematic signal overlap, enable higher stimulatory specificity, and perhaps lead to greater precision in both signal input and biological functional output.[2,6-11] However, for the proximate growth strategy to be effective, the tone dependent spatial arrangement of nerves must be preserved and will require directional control of regenerating neurites.[1] Moreover, since the nervous system depends on location specific signaling, similar spatial resolution limitations are anticipated for any device that interfaces with the nervous system.

Consequently, precise spatial neural regeneration will be crucial to realize the functional potential of next-generation neural prostheses.

Therefore, as a step toward enhanced neural prostheses performance, we are exploring the use of photopolymerization to fabricate micropatterns on biocompatible methacrylate polymers to support and guide neurite regeneration. Photopolymerization is a rapidly expanding biomaterials production platform due to its mild reaction conditions, high reaction rates at room temperature, and chemical versatility of monomer systems. The overall objective of the research is to translate fundamental photopolymerization methodology and understanding of nerve cell-material interactions into directed nerve regeneration that improves the ultimate performance of neural prosthetics.

EXPERIMENTAL

Glass substrate methacrylation. Standard glass microscope slides were functionalized with a silane coupling agent to prevent delamination of the polymer from the glass during sample characterization and cellular studies. Prior to treatment with the coupling agent, slides were first cleaned and oxidized with O_2 plasma for 3 min at 30 W RF power (PDC-001 Harrick Plasma Expanded Cleaner, Ithaca, NY) while under 300 mTorr vacuum. Immediately following removal from the plasma chamber, the slides were immersed in a 1/100 v/v solution of 3-(trimethoxysilyl)propyl methacrylate (Aldrich) and n-hexane (Aldrich) and were left overnight in a covered container at room temperature (~21°C). Each slide was then rinsed with fresh hexanes and allowed to dry in a fume hood before being placed in a sealed container. Functionalized slides were immediately used for polymerization when removed.

Photopolymerization of micropatterned methacrylate thin films. Monomer mixtures of hexyl methacrylate (HMA, Aldrich), 1,6 – hexanediol dimethacylate (HDDMA, Aldrich) and hydroxyl ethyl methacrylate (HEMA, Aldrich) were prepared with 1 wt% of 2,2-dimethoxy-2- phenylacetophenone (DMPA, BASF) as the photoinitiator (Fig. 2). Copolymer compositions are represented as whole numbers (e.g. 40/60, 50/50) but each polymer fraction takes into account the 1 wt% for the photoinitiator. A volume of 20 µL from pre-polymer formulations was pipetted onto the center of a functionalized slide then covered with a 2.54 cm x 2.54 cm x 0.1 cm glass-chrome Ronchi rule photomask (Applied Image Inc., Rochester, NY) for parallel patterns or with a cut untreated glass slide of the same dimensions for unpatterned samples.

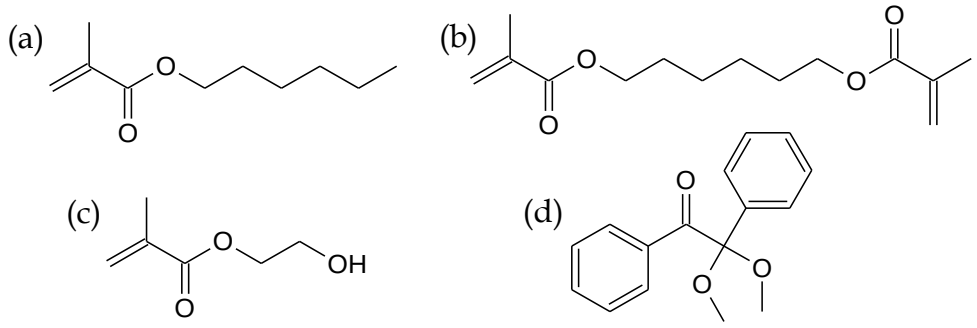

Figure 2. Chemical structures of monomers and photoinitiator used in methacrylate micropattern fabrication. Shown are (a) hexyl methacrylate (HMA), (b) 1,6-hexanediol dimethacrylate (HDDMA), (c) hydroxy ethyl methacrylate (HEMA), and (d) 2,2-dimethoxy-2-phenylacetophenone (DMPA).

Formulations spread evenly between the substrate and photomask. Photopolymerization was carried out with a high-pressure mercury vapor arc lamp (Omnicure S1500, Lumen Dynamics, Ontario, Canada) at a 365 nm light intensity of 16 mW/cm^2. Light intensity was measured with a Cole-Parmer Series 9811 radiometer. The curing module was equipped with an 8 mm aperture x 50 mm length beam homogenizing fused silica light pipe (Edmund Optics) and a collimating lens (RLQ-1, Asahi Spectra).

Microfeature amplitude was tuned by shuttering UV radiation at specific times to prevent further initiation events resulting in rapid termination of the polymerization. Following the set exposure time, the photomask was removed from the polymer and the sample was washed with 95% ethanol to remove residual surface monomer.

White light interferometry. Micropattern feature spacing and depth were measured by white light interferometry (Dektak Wyko 1100 Optical Profiling System, Veeco). Feature amplitude was measured as the difference between a maximum ridge value and an adjacent minimum groove value. For each composition and exposure time, average feature height was determined by measuring channel amplitude in nine different areas across the surface ($n \geq 3$). Feature spacing or periodicity was measured as the distance between the highest points on adjacent ridges and was consistent with photomask band spacing. Measurements and 3D images were generated using *Vision* software.

Scanning electron microscopy. Micropattern morphology of each composition was further characterized by scanning electron microscopy (SEM, S-4800, Hitachi). Conductive silver paint was applied to the bottom of glass substrates modified with micropattered methacrylate thin films for mounting on aluminum SEM stubs to acquire top-down images. For cross-sectional images, a glass etcher was used to etch the sample on the side opposite of the thin polymer film and patterned polymers were then fractured and mounted vertically on specimen stages. The SEM specimen stage was angled using automated stage and software controls. Each polymer surface was sputter coated with gold prior to examination by SEM. Electron accelerating voltage was set at 2 kV.

Photo-Differential Scanning Calorimetry (Photo-DSC). Kinetic measurements were made during the photopolymerization using differential scanning calorimetry (Perkin-Elmder, DSC). A 3 mg mixture of each methacrylate composition was deposited into a dimpled aluminum pan and photopolymerized at 30°C under the same lamp and light intensity as used for micropattern fabrication. A reference aluminum pan was placed in the reference holder of the instrument (Perkin-Elmer DSC). Light intensity of the high pressure mercury vapor arc lamp was tuned using shutter opening controls on the module. Maximum polymerization rate was calculated at the point of highest heat flow and double bond conversion was determined by integrating the polymerization rate profile. Design Expert 9 was used for design of experiment (DOE) modeling and analysis of kinetic data.

Spiral ganglion neuron cell culture. Dissociated SG cultures from 3-5 day old rat pups were prepared and plated as previously described.[12,13]

Quantification of neurite alignment. Total neurite length (T_L) was measured in Image J as previously described.[13] Aligned length (A_L), distance traveled only in the direction of the line-space grating, was similarly measured in Image J. Neurite alignment was subsequently calculated as a ratio of aligned length to total neurite length (A_L/T_L). Neurites that are strongly guided by the pattern have alignment ratios approaching one. Conversely, neurites that wonder, or do not strongly track microfeatures have much lower ratios. Neurites with alignment ratios close to one track micropattern feature direction throughout the majority of their length.

RESULTS AND DISCUSSION

Photopolymerization of micropatterns – Micro-features are generated across polymer surfaces by means of the spatial control of photopolymerization. Pre-polymer reaction mixtures are selectively exposed to UV irradiation through photomasks that have band spacing at size scales which are relevant to the cell (Fig. 3). Photomasks for parallel line-space gratings consist of alternating reflective (chrome) and transparent (glass) bands. During UV exposure, polymerization occurs rapidly under transparent bands that transmit full, incident light intensity from the source which results in raised ridges. Light that is diffracted after passing through the micro-scale transparent bands, and migration of reactive chains

during the reaction cause slow polymerization in areas under the reflective bands which results in surface depressions between raised features. As a result, a pattern of parallel micro-ridges and grooves of uniform width and amplitude rapidly develop across the substrate surface in a single fabrication step.

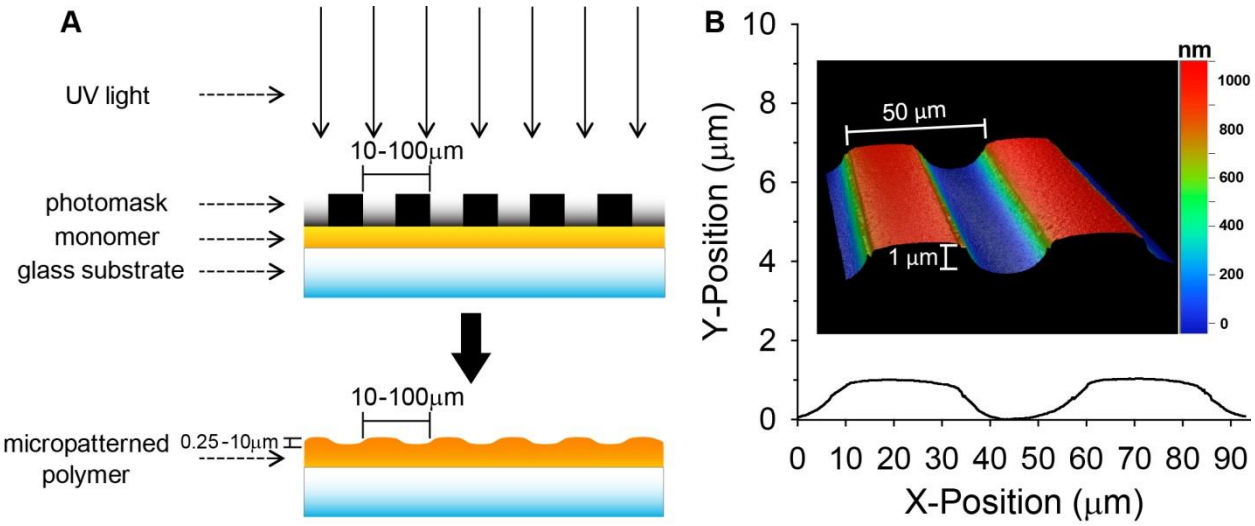

Figure 3. Photopatterning process schematic. **A)** Photoinitiator and monomer systems are selectively exposed to UV light through a photomask resulting in raised microfeatures across the surface. **B)** 2D Profile of micropatterned HMA-co-HDDMA with a periodicity of 50 μm and an amplitude of 1μm. *Inset*: 3D representation of a 100 μm^2 area derived by white light interferometry.

Tunable surface features –Surface features are readily tuned by altering simple parameters of the photopolymerization. Namely, control over feature height is achieved by changing reaction parameters such as initiator concentration and species, light intensity, and UV exposure time (Figs 4-5). For example, maximum feature amplitude was increased by 50% from 8 μm to 12 μm at low DMPA concentrations (data not shown). However, micropatterns cured with BAPO as the photoinitiator showed the opposite trend with high maximum amplitudes being captured with higher initiator content. For the HMA-co-HDDMA system, absolute feature height is tuned by approximately two orders of magnitude ~100 nm – 10 μm (results are only shown for 1-10μm regime).

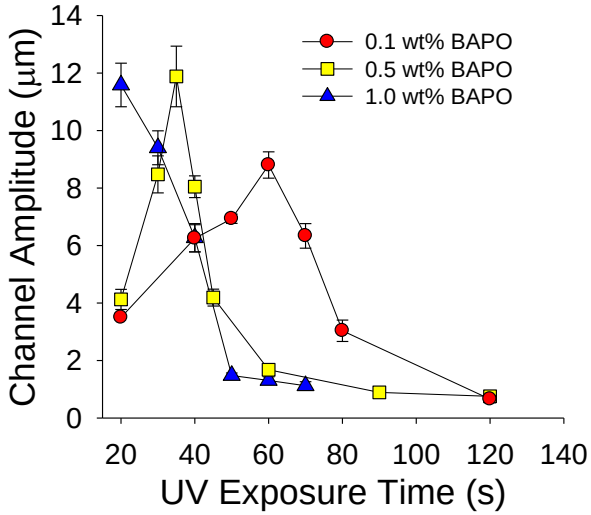

Figure 4. Micropattern feature height is tuned by modulating photoinitiator concentration and species and by varying UV exposure time. Increasing BAPO photoinitiator concentration shifted amplitude profiles to smaller time steps and increased maximum attainable amplitude by 50%. Photomask band spacing was 25 μm and a 16mW/cm^2 light intensity at 365 nm was used.

Increases in light intensity raised reaction rates and shifted final amplitude profiles to earlier time steps and also decreased the maximum attainable amplitude for microfeatures which was likely due to decreases in diffusion of reactive species caused by faster polymerization rates (Table 1). Feature spacing is controlled based on pattern dimensions in the photomask. However, the maximum feature height that could be attained for a given photoinitiator concentration and light intensity is limited by diffraction of light as it passes through photomask bands and by diffusion of reactive species that migrate more readily into shadowed areas as band space decreases (Table 2).

365 nm Light Intensity (mW/cm^2)	Max Amplitude (μm)	t_{max} (s)
8	8.09 ± 0.55	90
15	8.24 ± 0.69	79
19	7.91 ± 0.40	75
24	7.86 ± 0.25	71
55	7.27 ± 0.25	64
80	6.71 ± 0.23	58

Table 1. Modulation light intensity and photomask band spacing modify micropattern formation. Increasing light intensity tightens the channel amplitude vs. exposure time profile and shifts it to lower time steps.

Mask Periodicity (μm)	Max Amplitude (μm)	t_{max} (s)
10	1.81 ± 0.07	76
33	5.72 ± 0.36	76
50	8.21 ± 0.65	76
100	10.75 ± 1.09	76

Table 2. Photomask band spacing modify micropattern formation. Diffraction of light and diffusion of reactive species limit the maximum amplitude that can be obtained under given reaction conditions.

Micropattern characterization by SEM – In addition to characterization by white light interferometry, SEM was used to confirm microfeature dimensions and homogeneity (Fig 5). 3D angled side views demonstrate that parallel ridges and grooves extend across the substrate surface and that the features are homogenous, excluding edge effects. The smooth transitions between micro-features on the substrate surface are distinctly different from sharp features generated by etch or imprint lithography.

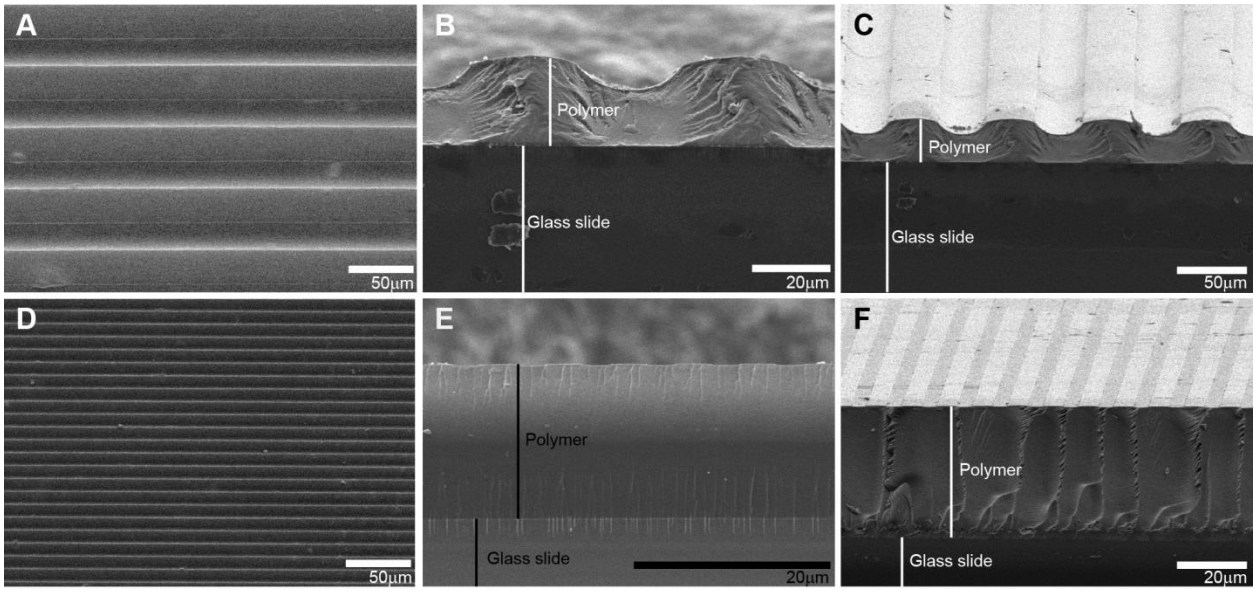

Figure 5. Representative SEM images of micropatterned HMA-co-HDDMA polymers. **A-C)** SEM images are shown of a pattern with a 50 μm periodicity and a channel amplitude of 8 μm. **D-F)** SEM images are shown of a pattern with a 10 μm periodicity and a channel amplitude of 250 nm. Top down view (A),(D); Cross-sectional view (B),(E); Angled cross-sectional view (C),(F). Note the gradual transitions between ridges and grooves.

Studying nerve or general cell contact guidance on gradually sloping features remains largely unexplored and may provide additional insight into cellular mechanisms that provide a causal response to surface features. Additionally, sloping features enable delicate biochemical studies that probe the effects of pharmacological agents on neurite guidance which may otherwise be difficult to explore with the potentially masking effects of sharp or 'infinite' slope features.

Kinetics of methacrylate photopolymerization – A tri-component mixture design of experiments (DOE) was used to model and predict basic reaction kinetics of methacrylate monomer mixtures relevant to neuronal contact guidance studies. Response surface models were generated and analyzed for maximum rate of propagation (R_p), time to reach maximum rate, and double bond conversion. The response surfaces will be used in conjunction with further work to understand reaction kinetic effects on micro-feature formation during masked photopolymerization. Developing a model that relates polymerization reaction kinetics to controllable micro-features, then it would be a powerful tool and predictor for fabrication of contact guidance substrates for future cell-material interaction studies.

Lattice Pt	HMA	HDDMA	HEMA
1	1	0	0
2	0	1	0
3	0	0	1
4	0.667	0.333	0
5	0.333	0.667	0
6	0	0.667	0.333
7	0	0.333	0.667
8	0.333	0	0.667
9	0.667	0	0.333
10	0.334	0.334	0.333
11	0.5	0.25	0.25
12	0.25	0.5	0.25
13	0.25	0.25	0.5

Table 3 – Lattice points (1-10) and checkpoints (11-13) for tri-component mixture experiments for DOE analysis and modeling.

Max Rate of Propagation - R_p

The max R_p was determined from DSC measurements using the following equation:

$$R_p = Q\left(\frac{M_1}{x_1 m_T n_1 \Delta H_{pol}} + \frac{M_2}{x_2 m_T n_2 \Delta H_{pol}} + \frac{M_3}{x_3 m_T n_3 \Delta H_{pol}}\right)$$

R_p = rate of propagation (s^{-1})
Q = heat released during polymerization (W)
$M_{1,2,3}$ = molecular weight of each monomer species (g/mol)
$x_{1,2,3}$ = fraction of sample mass for each monomer species
m_T = total sample mass used in DSC measurements (g)
$n_{1,2,3}$ = number of double bonds available for polymerization on each monomer
ΔH_{pol} = enthalpy of polymerization (J/mol)*

*Heat of polymerization was assumed to be a general methacrylate value of 54.8 kJ/mol for each monomer species.[14] Maximum R_p was measured as a system response as it may play a crucial role in the development and control of micropattern fabrication using masked photopolymerization.

The suggested special quartic model gave the best statistical fit for the Max R_p data with an F-value of 165.24. The measure of signal to noise ratio – Adeq Precision – is much greater than 4, at 36.14, illustrating that the response in relation to the error is significant. The adjusted R-squared value for the special quartic model is 0.9835 indicating a strong fit.

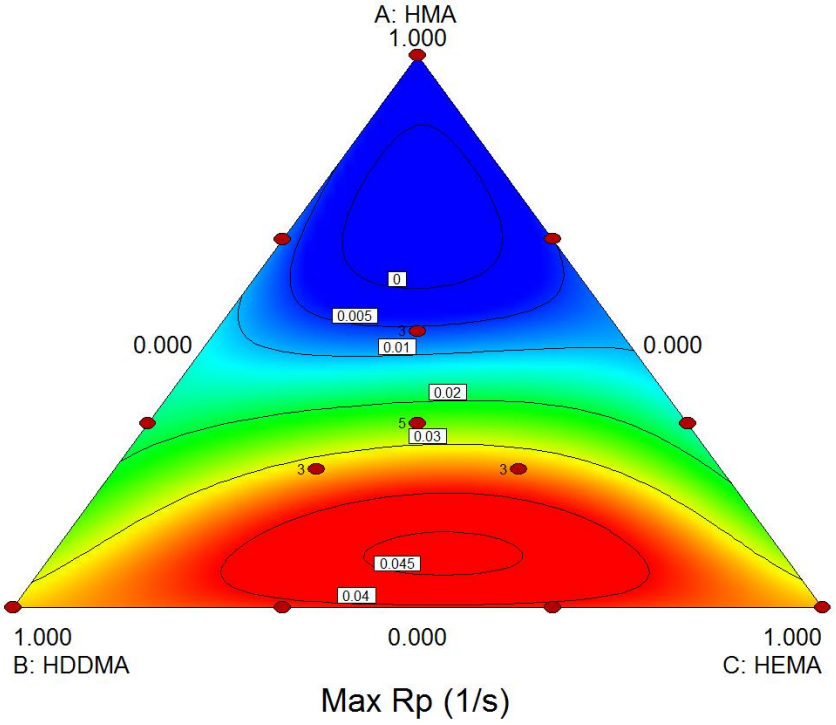

Figure 6 – Tri-component mixture response surface of max R_p for HMA-HDDMA-HEMA mixtures

The special quartic model equation developed for Max R_p is:

$$\text{Max } R_p = 2.919*10^{-3}\mathbf{A} + 0.032\mathbf{B} + 0.033\mathbf{C} - 0.023\mathbf{AB} - 0.037\mathbf{AC} + 0.026\mathbf{BC} - 1.27\mathbf{A^2BC} + 0.71\mathbf{AB^2C} + 1.04\mathbf{ABC^2}$$

The highest values of polymerization rate are obtained with using a fairly even ratio of HDDMA to HEMA and little if any HMA (Fig 6). It should be noted that HMA has very low max R_p values principally because it does not undergo auto-acceleration under the given conditions. Auto-acceleration occurs in radical polymerization when system vitrification becomes high enough as to inhibit biradical termination but low enough to allow monomer diffusion to propagating kinetic chains. As a consequence of inhibited termination reactions, R_p dramatically increases prior to its subsequent rapid decrease once propagation reactions become strongly inhibited by the viscosity of the system. Neat HDDMA increases quickly in viscosity, and thus undergoes auto-acceleration, since it is a difunctional methacrylate and undergoes cross-linking. While HEMA is only a mono-functional methacrylate, the hydroxyl group on each monomer enables the system to undergo pseudo-crosslinking with the continued formation and breaking of hydrogen bonds. Accordingly, it also undergoes a strong auto-acceleration effect. The model appears to strongly fit the physical phenomenon observed through DSC experiments.

Based on the equation coefficients, the concentration of HDDMA and HEMA have a much more significant effect on Max R_p than does that of HMA. It should be noted, that the complex quartic interaction terms have the largest coefficients illustrating that response is not solely additive, but that the interactions between monomers in the pre-polymer formulation are also significant.

Time to max R_p

In addition to the actual max R_p, the time required to reach the max may also be relevant to generation and control of photopolymerized microfeatures. Accordingly, the time to max R_p was measured during each of the DSC experimental runs (Fig 7).

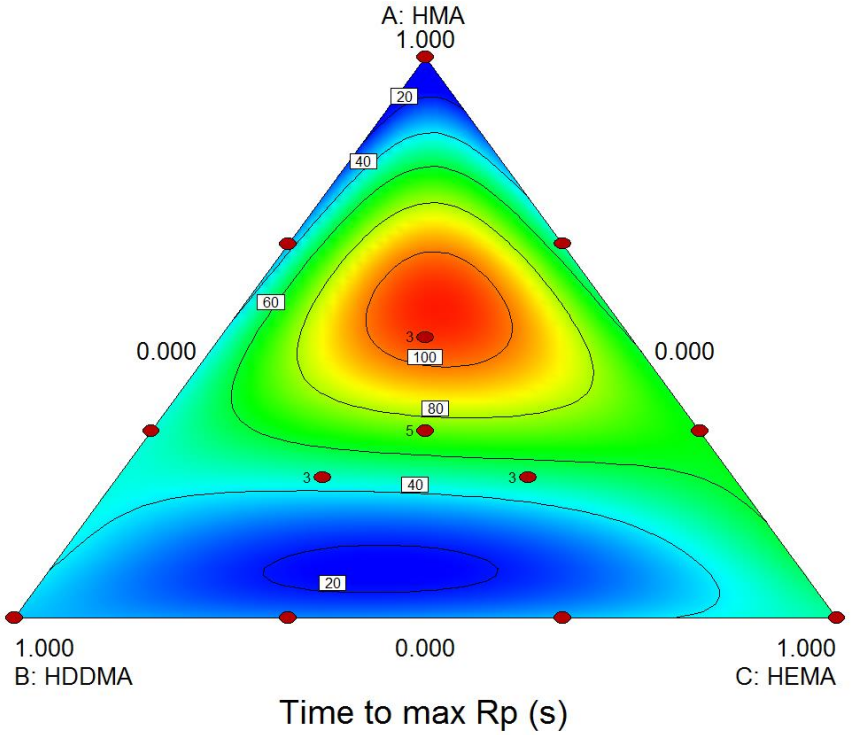

Figure 7 – Tri-component mixture response surface of time to reach max R_p for HMA-HDDMA-HEMA mixtures

As with the model for max R_p, a special quartic model gave the best statistical fit for the given data with an F-value of 10.37. There is only a 0.01% chance that the model occurs due to noise. The measure of signal to noise ratio – Adeq Precision – is greater than 4, at 12.42, illustrating that the response in relation to the error is significant. The adjusted R-squared value for the special quartic model is 0.773 indicating a relatively good fit, but not as strong as that seen for the max R_p model.

The special quartic model equation developed for Time to max R_p is:

$$T_{max}\ R_p\ (s) = 4.6\mathbf{A} + 36.29\mathbf{B} + 49.68\mathbf{C} - 82.83\mathbf{AB} - 127.02\mathbf{AC} - 44.48\mathbf{BC} + 5598.44\mathbf{A^2BC} - 1769.61\mathbf{AB^2C} - 1862.68\mathbf{ABC^2}$$

DOE methodology is a particularly valuable tool to determine response directionality. Based on a relatively low number of experiments, a 'sweet spot' with defining contours can be determined for both long and short times to reach max R_p. Since HDDMA undergoes auto-acceleration most quickly due to its effects on viscosity as a crosslinker, the higher its concentration the faster the mixture reaches its max R_p. HMA also reaches max Rp very quickly, but it should be noted that its max was on the order of 5-10X lower than that seen for neat HDDMA and HEMA systems. HMA reaches max R_p very early on in the reaction and does not undergo the radical polymerization auto-acceleration effect which would delay onset on the maximum propagation rate. Accordingly, max R_p takes longer to achieve with increasing

concentrations of HMA until the system becomes sufficiently linear (i.e. lacking covalent HDDMA cross-links or pseudo HEMA crosslinks) as to prevent auto-acceleration. Thus, a global maximum, for this particular tri-component mixture, is observed near the 50 HMA 25 HDDMA 25 HEMA point used in the initial model generation.

Based on the equation coefficients, the concentration of HDDMA and HEMA have a much more significant effect on Time to max R_p than does that of HMA. It should be noted, that the complex quartic interaction terms have, by far, the largest coefficients illustrating that response is not solely additive, but that the interactions between monomers in the pre-polymer formulation is also significant. In this case, the interaction terms so thoroughly dwarf the linear terms that they could be excluded if not for the hierarchy rule to generate the model.

Methacrylate Double Bond Conversion

Conversion was determined by calculating the area under the R_p curve using the trapezoidal rule. It is assumed that conversion will also play a significant role in the observed feature dimensions generated through masked photopolymerization. Accordingly, its response for the DOE tri-component response surface analysis was also measured (Fig 8). In contrast to the models suggested for Max R_p and Time to max R_p, a cubic model gave the best statistical fit for the given data with an F-value of 27.84. The measure of signal to noise ratio – Adeq Precision – is greater than 4, at 18.78, illustrating that the response in relation to the error is significant. The adjusted R-squared value for the special quartic model is 0.917 indicating a strong fit.

The cubic model equation developed for conversion is:

Conversion = 0.26**A** + 0.59**B** + 0.74**C** + 0.43**AB** + 0.31**AC** – 0.28**BC** + 4.57**ABC** – 0.94**AB(A-B)** – 1.58**AC(A-C)**

Increasing HEMA concentration generally correlates with an increased final conversion of the given tri-component system (Fig 8). It is likely that HDDMA cannot reach as high of a conversion as predominantly HEMA mixtures due to rapid vitrification caused by covalent cross-links. In contrast, HEMA still undergoes a strong auto-acceleration affect, but propagating species are not trapped as early in the reaction due to the transitory nature of the pseudo-crosslinks (i.e. hydrogen bonds) in the HEMA network. Double bond conversion is low for mixtures that are predominantly HMA in concentration.

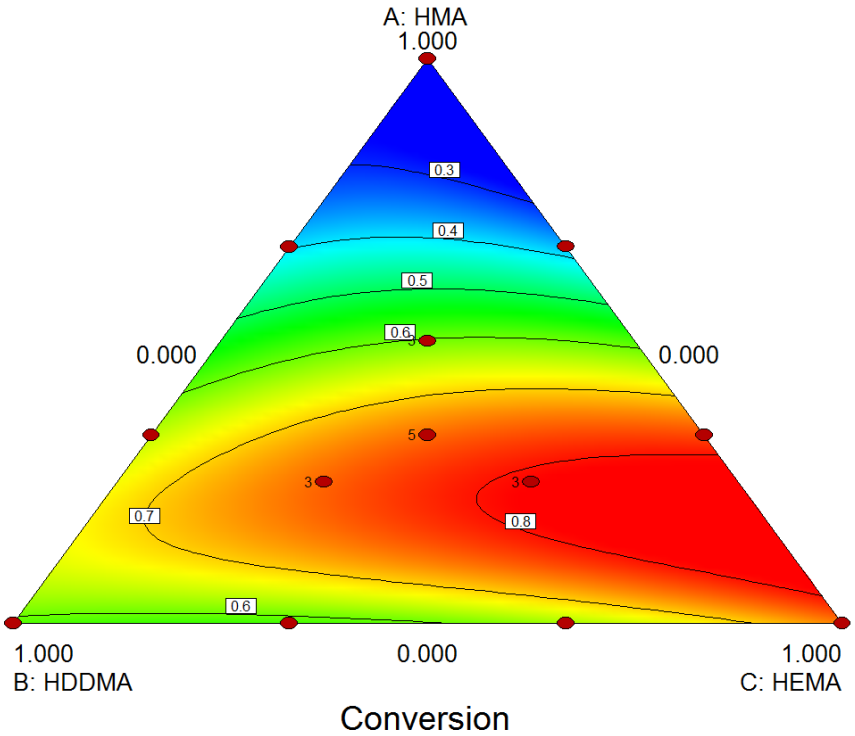

Figure 8 – Tri-component mixture response surface of polymer conversion for HMA-HDDMA-HEMA mixture

Based on the equation coefficients, the concentration of HDDMA and HEMA have a more significant effect on conversion than does that of HMA. However, the interaction factors, particularly that between all three monomer species (**ABC),** is the strongest contributing factor to the final conversion outcome. The equation again illustrates that the response is not solely additive, but that the interactions between monomers in the pre-polymer formulation is very significant.

Inner ear nerve cells orient to surface features – Spiral ganglion neurons (SGNs), inner ear nerve cells, were cultured on 40/60 wt% poly(HMA-co-HDDMA) parallel line-space gratings and on unpatterned samples as a control. Neurites were visualized with an epi-fluorescent microscope and measured using Image J. Dissociated SGNs cultured on unpatterned substrates extended regenerating neurites in random directions across the polymer surface (Fig 9A). However, regenerating neurite outgrowth was strongly oriented in the direction of the micro-features (horizontal) when SGNs were cultured on patterned substrates (Fig 9B). Additionally, neurites encountering the pattern at a steep angle relative to the features were caused to turn and follow the direction of the pattern after short distances. SGN neurites, therefore, respond and orient to gradually sloping features formed by the described patterning photopolymerization method.

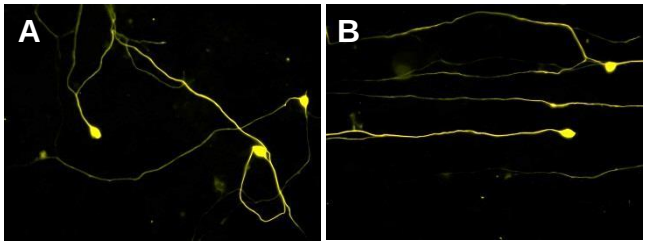

Figure 9. Dissociated SGN neurite growth on unpatterned or patterned 40/60 wt% poly(HMA-co-HDDMA). A) Neurite growth is random on unpatterned substrates. B) Regenerative growth runs parallel to micropattern features (horizontal) with 25 μm spacing and an 8 μm height. SGNs were immunostained with anti-NF200 antibody (yellow).

Tuning extent of neurite alignment – For line-space grating patterns, SGN neurite alignment was measured as the ratio of aligned distance per length of neurite (A_L/T_L). The closer the ratio is to one the more aligned the entire neurite is to the pattern features. To explore the effect of channel amplitude on SGN neurite orientation, pattern pitch was kept constant at 50 μm and channel amplitude was varied from 1 to 8 μm by shuttering the UV radiation source at specific time steps during the reaction. The extent of SGN neurite orientation to feature height significantly increases with increasing channel depth (Fig 10A).

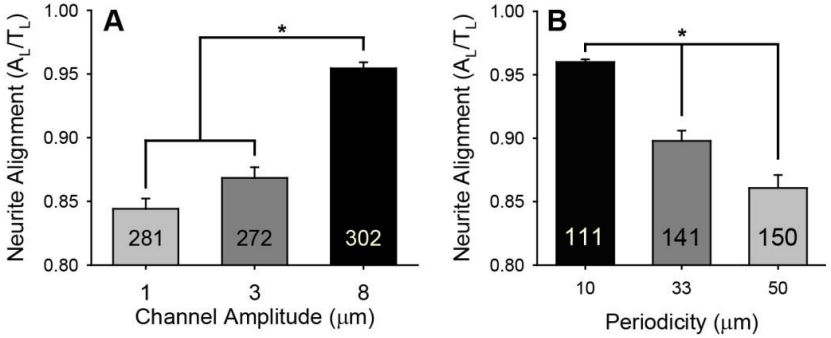

Figure 10. SGN neurite alignment to line-space gratings depends on channel depth and periodicity. Neurite alignment was measured as a ratio of total neurite length minus aligned length divided by total length (A_L/T_L). Ratios that approach one indicate the highest degree of alignment. **A)** SGN neurite alignment increased significantly with increasing channel depth ($p<0.05$, KW ANOVA). **B)** SGN neurite alignment was also shown to significantly increase with decreasing feature spacing while maintaining feature height at 1 μm ($p<0.05$, KW ANOVA). * Indicates that the group is different from all others ($p<0.05$).

Feature frequency also significantly affected the total extent of directed neurite regeneration. Channel amplitude was maintained at 1 μm and cells were cultured on patterns with periodicities of 10, 33, and 50 μm. SGN neurite alignment significantly increased with increasing feature frequency (Fig 10B). Interestingly, orientation on a 10μm periodicity 1 μm amplitude sample was not statistically different from SGN neurite orientation on a 50 μm periodicity and 8 μm amplitude.

CONCLUSION

The described research presents a radiation curing method to generate physical micropatterns in biomaterials and demonstrates the first use of topographic cues to align neurites of neurons from the inner ear. It is anticipated that the results of this interdisciplinary effort will contribute significantly to polymer neural regeneration technology and will lead to novel clinical techniques to improve CIs and, consequently, the quality of life for CI patients. Further, the knowledge gained about peripheral nervous system growth on these engineered biomaterials may improve existing or future therapies to treat PNS damage and may also enhance other facets of tissue engineering.

ACKNOWLEDGEMENTS

The authors would like to acknowledge the National Center for Research Resources (NCRR) (grant number UL1RR024979), a part of the National Institutes of Health (NIH), and the American Hearing Research Foundation (AHRF) for project funding. We also acknowledge funding from the Department of Defense for a National Defense Science and Engineering Graduate (NDSEG) research fellowship awarded to the presenting author.

REFERENCES

1. O'Leary, S. J.; Richardson, R. R.; McDermott, H. J. Principles of design and biological approaches for improving the selectivity of cochlear implant electrodes. *Journal of Neural Engineering* **2009**, *6*, 055002.

2. Leng, T.; Wu, P.; Mehenti, N. Z.; Bent, S. F.; Marmor, M. F.; Blumenkranz, M. S.; Fishman, H. A. Directed retinal nerve cell growth for use in a retinal prosthesis interface. *Invest. Ophthalmol. Vis. Sci.* **2004**, *45*, 4132-4137.

3. Winter, J. O.; Cogan, S. F.; Rizzo,Joseph F.,,III Retinal prostheses: current challenges and future outlook. *Journal of Biomaterials Science-Polymer Edition* **2007**, *18*, 1031-1055.

4. Shannon, R. V.; Fu, Q. J.; Galvin, J.,3rd The number of spectral channels required for speech recognition depends on the difficulty of the listening situation. *Acta Otolaryngol. Suppl.* **2004**, *(552)*, 50-54.

5. Rubinstein, J. T. How cochlear implants encode speech. *Curr. Opin. Otolaryngol. Head Neck Surg.* **2004**, *12*, 444-8.

6. Evans, A. J.; Thompson, B. C.; Wallace, G. G.; Millard, R.; O'Leary, S. J.; Clark, G. M.; Shepherd, R. K.; Richardson, R. T. Promoting neurite outgrowth from spiral ganglion neuron explants using polypyrrole/BDNF-coated electrodes. *Journal of Biomedical Materials Research Part a* **2009**, *91A*, 241-250.

7. Brors, D.; Aletsee, C.; Schwager, K.; Mlynski, R.; Hansen, S.; Schäfers, M.; Ryan, A. F.; Dazert, S. Interaction of spiral ganglion neuron processes with alloplastic materials in vitro. *Hear. Res.* **2002**, *167*, 110-121.

8. Mehenti, N. Z.; Peterman, M. C.; Leng, T.; Marmor, M. F.; Blumenkranz, M. S.; Bent, S. F. A retinal interface based on neurite micropatterning for single cell stimulation. *Invest. Ophthalmol. Vis. Sci.* **2003**, *44*, U704-U704.

9. Roehm, P. C.; Hansen, M. R. Strategies to preserve or regenerate spiral ganglion neurons. *Curr. Opin. Otolaryngol. Head Neck Surg.* **2005**, *13*, 294-300.

10. Guenther, E.; Troger, B.; Schlosshauer, B.; Zrenner, E. Long-term survival of retinal cell cultures on retinal implant materials. *Vision Res.* **1999**, *39*, 3988-3994.

11. Cui, X. Y.; Wiler, J.; Dzaman, M.; Altschuler, R. A.; Martin, D. C. In vivo studies of polypyrrole/peptide coated neural probes. *Biomaterials* **2003**, *24*, 777-787.

12. Tuft, B. W.; Li, S.; Xu, L.; Clarke, J. C.; White, S. P.; Guymon, B. A.; Perez, K. X.; Hansen, M. R.; Guymon, C. A. Photopolymerized microfeatures for directed spiral ganglion neurite and Schwann cell growth. *Biomaterials* **2013**, *34*, 42-54.

13. Clarke, J. C.; Tuft, B. W.; Clinger, J. D.; Levine, R.; Figueroa, L. S.; Allan Guymon, C.; Hansen, M. R. Micropatterned methacrylate polymers direct spiral ganglion neurite and Schwann cell growth. *Hear. Res.* **2011**, *278*, 96-105.

14. Lee, H.; Colby, C. Heat of polymerization of nine mono-, di-, and trimethacrylate esters tested neat and with low levels of peroxide by dynamic differential scanning calorimetry. *Dental Materials* **1986**, *2*, 175-178.